Impact of Friction and Scale-Dependent Initial Stress on Radiated Energy-Moment Scaling

Bruce E. Shaw

Lamont–Doherty Earth Observatory, Columbia University, New York, USA

The radiated energy coming from an event depends on a number of factors, including the friction and, crucially, the initial stress. Thus we cannot deduce any scaling laws without considering initial stress. However, by simulating long sequences of events, where the system evolves to a statistically steady-state, we can obtain the appropriate distribution of initial stresses consistent with the dynamics and a given friction. We examine a variety of frictions, including power-law slip dependence, and explore a variety of scaling relations, with the aim of elucidating their radiated energy-moment scaling. We find, contrary to expectations, that apparent stress is not seen to increase with earthquake size for power-law weakening. For small and for large events, little change in apparent stress is seen with increasing rupture size, while intermediate sized events interpolate in between. We find the origin of this unexpected lack of size dependence in systematic changes of initial stress, with bigger events tending to sample regions of lower initial stress. To understand radiated energy-moment scaling, scale-dependent initial stress needs to be considered.

1. INTRODUCTION

Whether radiated energy scales linearly with moment, or has some nonlinear scaling is an open and important question. Observationally, a number of authors have come to quite different conclusions, with some arguing for a nonlinear dependence [*Kanamori et al*., 1993; *Abercrombie*, 1995; *Mayeda and Walter*, 1996; *Prejean and Ellsworth*, 2001; *Wu*, 2001; *Richardson and Jordan*, 2002; *Stork and Ito*, 2004] while others argue for a linear dependence [*McGarr*, 1999; *Ide and Beroza*, 2001]. Theoretically it is an important question because different scalings have different implications for what physics might be controlling the earthquake source [*Shaw*, 1998].

Certainly, linear scaling need not hold. *Abercrombie and Rice* [2005], motivated by observations which they take to support a nonlinear scaling, have also tried to work backwards to infer a slip-weakening friction which would reproduce a power-law nonlinear scaling. They proposed a power-law slip-weakening friction, and argued based on fracture energy considerations that this should reproduce a power-law radiated energy-moment scaling. Yet because the energetics of the problem also involve the initial stress into which the rupture propagates, such an argument may not necessarily hold in practice. Here, we study power-law weakening frictions numerically to examine what kinds of radiated energy-moment scaling does result. We look at the stress fields both before, during, and after the ruptures to get fuller constraints on the energetics. We find nonlinear scaling not predicted by arguments which neglect the underlying heterogeneity of the stress field. In order to understand the energy radiated by earthquakes, and how it scales with rupture size, we need to consider how all the sources and sinks of energy scale with rupture size in the problem. In this paper, we point to a hitherto neglected scaling with earthquake size of one of the sources, the

Earthquakes: Radiated Energy and the Physics of Faulting
Geophysical Monograph Series 170
XXXXXXXXXXXXXXXXXXXXXXXXXXX
10.1029/170GM27

initial energy available for rupture, reflected in the initial stress below the threshold breaking stress.

The paper is organized as follows. We present briefly the numerical model we use, and the techniques we have developed for measuring radiated energy. We then present radiated energy-moment scaling relations for a range of power-law frictions, including slip-weakening and velocity-weakening friction. Next, we examine a series of other scaling laws to seek insight into the unexpected radiated energy-moment scaling found. Looking into the stress fields involved, we find evidence which helps explain some of the counterintuitive scaling seen for small events. Readers uninterested in the model details may skip to the results section, and refer back to the model later if needed.

2. MODEL

We use a two dimensional scalar elastodynamic model in the geometry introduced by *Shaw* [2003]. This has the advantage of allowing radiating boundary conditions far from the fault to minimize reflections, as well as including the effective coupling of the stably sliding lower fault through a traction on the unstably sliding seismogenic fault boundary. With the lower dimensional model we can study higher numerical resolutions on large domains over long sequences of events. This allows self-consistent initial stress conditions, leftover from previous events, to develop. Plate 1 illustrates the geometry of the problem, showing a snapshot of the heterogeneous displacement field which has developed after many events have occurred.

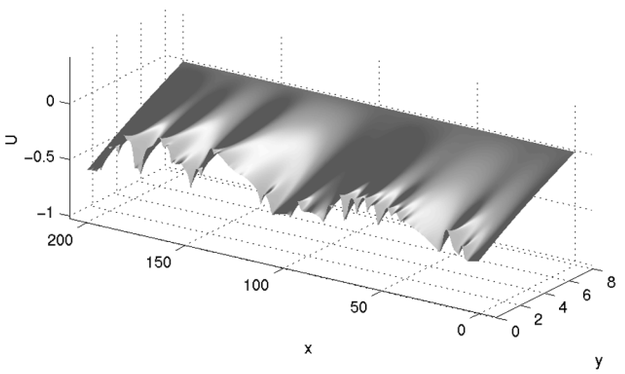

Plate 1. Geometry of the model fault. Surface plot of displacement U on the fault, at $y = 0$, and in the two-dimensional interior, for $y > 0$. For this stuck static configuration, the interior smoothly interpolates from the boundary, being a harmonic solution of the Laplacian. Along the boundary, away from the fault, at $y = 8$ here, we use a radiating boundary condition during events [*Shaw*, 2003].

The model satisfies a scalar wave equation for the displacement field U in a two-dimensional (numerically finite) half-space:

$$\frac{\partial^2 U}{\partial t^2} = \nabla^2 U \tag{1}$$

for t time and the Laplacian $\nabla^2 = \frac{\partial^2}{\partial x^2} + \frac{\partial^2}{\partial y^2}$. We consider a rectangular geometry with x taken to be the distance parallel to the fault and y the distance perpendicular to it. We use dimensionless units throughout, to minimize the number of parameters. Here we have, for example, set the speed of sound to unity. To aid the reader in comparing our results against observations, we have added a conversion table back to dimensionful units in the Appendix. On the fault, located at $y = 0$, the tractions T balance the strain

$$\left.\frac{\partial U}{\partial y}\right|_{y=0} = T \tag{2}$$

The tractions consist of two parts, a friction τ_F, which we will discuss shortly, and the coupling to the stable sliding parts of the fault below the seismogenic layer

$$T = \tau_F + (vt - U) \ . \tag{3}$$

Here $v \ll 1$ is the slow plate velocity, and we have scaled lengths so the coupling stiffness is unity, so lengths scale with the seismogenic depth of unity. This second term coupling the plate displacement vt to the displacement on the fault U comes from a collapse of three dimensional effects onto our two dimensional problem. The interesting dynamics in the problem arises fundamentally from the friction, the term we turn to now.

Friction

All of the nonlinearity in the problem is contained in the friction τ_F, which has a stick-slip form, resisting motion up to some threshold value, and acting against motion when sliding occurs. We represent the stick-slip by

$$\tau_F = \Phi(\frac{\partial D}{\partial t'}, t' \le t) H(\frac{\partial D}{\partial t}) \tag{4}$$

where Φ is a scalar frictional strength, D is the slip and $\partial D/\partial t$ is the slip rate on the fault, and H is the antisymmetric step function

$$H = \begin{cases} \frac{\partial D}{\partial t} & \neq 0; \\ |H| < 1 & \frac{\partial D}{\partial t} = 0. \end{cases} \tag{5}$$

which represents the stick-slip nature of the friction being multivalued at zero slip rate, and opposing motion in the $\frac{\partial D}{\partial t}$ unit direction when slipping.

What remains a big open question for earthquakes, is what is the frictional strength τ_F. While there are reasons for thinking we may have a pretty good description of friction at slow slip rates [*Dieterich*, 1994; *Heslot et al.*, 1994], at high slip rates things are extremely uncertain; many potential physical effects may be occurring, with substantially different implications for friction, [*Sibson*, 1973; *Melosh*, 1996; *Rice*, 1999; *Tullis and Goldsby*, 2003.] With friction at high slip rates being an open question, we use a friction which has a minimum of parameters, is computationally efficient, and spans a range of frictional instabilities, including slip-, time-, and velocity- weakening [*Shaw*, 1995; *Shaw and Rice*, 2000]. We generalize a friction we have considered before [*Shaw*, 19975; *Shaw and Rice*, 2000] to have a power-law weakening, to explore the hypothesis of *Abercrombie and Rice* [2005].

For the friction, we consider five terms

$$\Phi = \Phi_0 - \frac{\alpha Q}{1+\alpha Q} - \frac{\beta Q^\eta}{1+\beta Q^\eta/\sigma} - \Sigma_t - \varepsilon \nabla_{\|}^2 \frac{\partial D}{\partial t} \qquad (6)$$

The first term Φ_o is a constant threshold. We could consider a spatially heterogeneous term here, $\Phi_o = \Phi_o(x)$, but the dynamics turns out to be invariant with respect to this term, as long as it is constant in time; only stress drops matter, not absolute stress [*Shaw*, 2004]. So, this Φ_o term is irrelevant to the problem.

The next term, which is a function of heat Q, models frictional weakening from frictional heating; pore fluid effects [*Sibson*, 1973; *Lachenbruch*,1980; *Shaw*, 1995] and flash heating of asperities [*Rice*, 1999; *Beeler and Tullis*, 2003] are two potentially relevant physical mechanisms which this simplified quantification could represent. Frictions with this functional form have been derived from physical effects [*Shaw*, 1995; *Beeler and Tullis*, 2003].

For the third term, to consider power-law weakening, we add a term like the second term, dependent on Q, but generalize it to having an exponent of η which is not necessarily unity. This generalization is not derived from a physical mechanism, but rather is postulated in order to study power-law weakening with $\eta < 1$. As noted previously in the case when $\eta = 1$, the weakening rate constant α plays a critical role in terms of distributions of sizes of events, while the results are relatively insensitive to the weakening parameter β [*Shaw and Rice*, 2000]; this also generalizes to the $\eta < 1$ case here.

Heat accumulates with slip rate, and dissipates over some timescale $1/\gamma$:

$$\frac{\partial Q}{\partial t} = -\gamma Q + \left|\frac{\partial D}{\partial t}\right|. \qquad (7)$$

Slip-weakening results from $\gamma \ll 1$, while velocity-weakening results from $\gamma \gg 1$ [*Shaw*, 1995]. Thus, using small γ, we can study the power-law slip weakening friction proposed by [*Abercrombie and Rice*, 2005]. (See that paper for a fuller discussion of what power-law slip-weakening looks like, and further motivations for studying it.)

The fourth term in Equation (6)

$$\Sigma_t = \begin{cases} \sigma_0 \dfrac{t - t_s}{t_0} & t - t_s < t_0; \\ \sigma_0 & t - t_s \geq t_0 \ . \end{cases} \qquad (8)$$

is a friction drop associated with nucleation, which we make a big simplification of and consider as a time-weakening term. It weakens with time t over a timescale t_0 since beginning slipping at t_s, and restrengthens when resticking occurs. This allows for a huge numerical speedup compared with more expensive rate and state formulations, both by compressing the nucleation phase into the finite timescale t_0 and allowing the limit of loading rate $v = 0$ to be taken. It also allows the study of time-weakening friction. It is not, however, without cost, and short time correlations between events such as aftershocks are not accounted for by this friction. Nevertheless, it does allow for our numerical time costs to be dominated by the regime of most interest to the dynamic rupture timescale. And, as we will show later, the results we will present are insensitive to this term.

The last term $\varepsilon \nabla_{\|}^2 \frac{\partial D}{\partial t}$, with ε a small constant and $\nabla_{\|}^2 = \partial^2/\partial x^2$ the fault parallel second derivative, provides stability at the shortest wavelengths for $\eta \geq 1$ [*Langer and Nakanishi*, 1993; *Shaw and Rice*, 2000], although as we will see it is insufficient at providing a continuum cutoff in the singular power-law $\eta < 1$ case.

The system is loaded until one point is just at the point of failure. The event evolves then under fully inertial dynamics. Once the event has stopped slipping, the waves are quenched in the system; then the system is reloaded until the next point is just at failure. This reloading is accomplished easily by calculating how far the static solution is from failure at every point, and then loading so the least stable point is just at failure. For simple geometries and frictions such as we have, this loading can be done analytically, while for more complicated geometries and frictions, numerical Green's functions can be used.

Parameters used in the simulations shown, unless otherwise indicated, are: domain parameters $\delta_x = .1$, $\delta_y = .0.5$, $L_x = 100$, $L_y = 8$; friction parameters $\alpha = 3$, $\gamma = .1$, $\beta = .1$, $\sigma = .3$, $\eta = .4$, $\sigma_0 = 0.1$, $t_0 = .1$, $\varepsilon = .0003$. These parameters

are chosen for the following reasons. For the grid resolution parameters δ_x and δ_y, we would like to make these as small as possible, but numerical costs scale as the cube of the grid resolution, so we are limited in how small we can make them. With $\delta_x = .1$ we have an order of magnitude resolution on the seismogenic lengthscale of unity in the fault parallel direction, so we are able to get a range of sizes of small events. The grid resolution perpendicular to the fault needs to be even more resolved than the fault parallel direction, and a factor of 2 has been seen to be sufficient for this additional resolution, hence $\delta_y = .05$. Fault parallel domain size L_x needs to be large enough so the longest events generally do not break the whole fault. Periodic boundary conditions are used along the fault. Fault perpendicular domain size L_y should be as large as possible, but numerical costs make this choice which is large compared to unity large enough so any imperfectly absorbed waves will not interfere with the dynamics on the fault. Radiating boundary conditions are used perpendicular to the fault [*Shaw*, 2004]. The friction parameter $\alpha = 3$ is chosen so as to get a rich population of small events [*Shaw and Rice*, 2000], The parameter $\gamma = .1$ is chosen to get slip weakening. The parameter $\beta = .1$ is not very important, in that a wide range of values of β will behave similarly. The parameter $\sigma = .3$ is chosen to be relatively large so that the power law weakening will dominate the stress drops for the small events, but not larger than the stress drop of unity coming from the α term so as to keep events localized and not all running away to be system sized events. The parameter η is chosen to be close to the exponent *Abercrombie and Rice* [2005] preferred from their data. The parameter σ_0 is chosen to be small so the nucleation term doesn't affect the stress drops, but not so small that we would be wasting numerical resources on tiny events. The parameter t_0 is chosen so the nucleation occurs on the timescale that the smallest events are resolved on the grid. The parameter $\varepsilon = .003$ is chosen to be large enough to give a continuum behavior when $\eta = 1$, but not too large that it affects larger scale events. Typical catalogue lengths are $vt \sim 100$ so that tens of repeat times of large events are simulated, corresponding to timescale of order thousands of years. Typical numbers of events in the catalogues are thousands to tens of thousand, with a wide range of event sizes.

The friction we use modifies a previously used friction by taking a drop in the state variable, the heat Q, and generalizing the drop to being a power law in Q. Thus the exponent $\eta = 1$ recovers the old friction. This generalized friction, while appealing from some theoretical points of view [*Abercrombie and Rice,*2005], presents a significant problem numerically: at low values of Q it is singular, with

$$\frac{\partial \Phi}{\partial Q} \sim Q^{\eta-1} \tag{9}$$

which diverges as $Q \to 0$ for $\eta < 1$. For slip-weakening friction, linear stability analysis shows unstable wavelengths scale as $\sqrt{\partial\Phi/\partial Q}$ while for velocity-weakening growth rates scale as $\sqrt{\partial\Phi/\partial Q}$. So neither of these frictions are properly resolvable numerically. We can solve our explicit finite difference numerical equations, but we do ultimately find grid resolution dependence quantitatively in the results. At the same time, since we find qualitative consistency in the results, we consider these qualitative features to be valid, with the caveat that some small scale physics we have not included in a continuum sense is implicitly being evoked out of the numerical grid. Unlike the behavior of slower weakening frictions for $\eta \geq 1$ which does have a well defined continuum limit [*Shaw and Rice*, 2000], this power law weakening $\eta < 1$ renders the problem "inherently discrete" [*Rice*, 1993].

3. RESULTS

Radiated Energy

We have measured radiated energy in two different ways and found agreement between the two methods. In one way, we use conservation of energy and infer the radiated energy [*Shaw*, 1998]. We measure potential energy before and after the event (after all the kinetic energy has been removed from the system), and the work done in sliding against friction on the fault. Then, for no dissipation in the bulk, by conservation of energy the radiated energy E_R will be the difference between the change in potential energy ΔPE and the work W done on the fault:

$$E_R = \Delta PE - W \tag{10}$$

where $W = \int \Phi dV d\Gamma$, $V = \partial D/\partial t$ is the slip rate, and Γ is the fault surface (so $d\Gamma = dx|_{y=0}$); and $PE = \frac{1}{2}\int (\nabla U)^2 dxdy$. We have also measured the radiated energy directly by looking at the flux of kinetic energy through a bounding surface S:

$$E_R' = \frac{1}{2}\int V^2 dtdS \tag{11}$$

This method is only approximately good in that we want to have the bounding surface be in the far field, and have time for all the energy to cross the field, but numerically we are constrained to finite distances and times. So for very large events we may be picking up some near field terms. Nevertheless, it works well in practice: Plate 2 shows a plot of radiated energy calculated in the two different ways plotted against each other, with E_R

measured from conservation of energy on the horizontal axis and E_R' measured from kinetic energy flux on the vertical axis. Only a slight excess of kinetic energy is seen for the largest events, reflecting this finite distance effect. Consistency of the two results shows the validity of our methodology.

Continuum Limit

Having established our methodology, we want to caution that the singularities in the friction we are using do not allow us to reach a continuum limit in the scaling. Finite frictions with $\eta = 1$ and finite slopes as $Q \rightarrow 0$ are resolved in a continuum limit sense, in that as $dx \rightarrow 0$ and $dy \rightarrow 0$ we obtain the same results at a given lengthscale L, as Plate 3a illustrates, where we plot the apparent stress $\tau_a = E_R/M$ [*Wyss and Brune*, 1968], the ratio of radiated energy E_R to moment M, versus the length of the rupture L for two different grid resolutions. Note here that the symbols basically overlay, so we indeed have a good continuum limit. In contrast, for $\eta < 1$ the unresolvable singularities as $Q \rightarrow 0$ leaves a residual dependence on grid resolution for $dx \rightarrow 0$ and $dy \rightarrow 0$, as Plate 3b illustrates. Now the different symbols do not overlay. This quantitative shift in the curves limits some of the things we can say. We will restrict ourselves, however, to answers which do not depend on these shifts. It is nevertheless important to keep these limitations in mind. (One last comment about this figure: the upward trend in τ_a for the small events in the continuum case Plate 3a is caused by an underlying increase in the static stress drop for the small events for the parameters used here. This is not important for the point we are addressing here about continuum behavior, but it does raise an issue we will need to consider later which is that to understand τ_a scaling we also must consider the static stress drop $\Delta\tau$.)

At the same time, while we do not have a good continuum limit in space, we do appear to have continuum time resolutions, and are not affected by nucleation issues. Numerically, smaller time steps do not affect our results. For the subtler question of how nucleation might be affecting things, Plate 4 shows that indeed nucleation is not affecting the results. We show two extremely different kinds of nucleation, one a time dependent nucleation with $\sigma_0 > 0$ and loading rate $v = 0$, and the other a continuous loading slip weakening nucleation with $\sigma_0 = 0$ and $v > 0$. Plate 4 shows that neither a change in parameter values nor this dramatic change in nucleation mechanisms affects the results. Thus the unexpected small event scaling of τ_a we will be discussing is not a nucleation issue.

Radiated Energy Scaling

We begin our results with a compendium of radiated energy versus moment scaling for a wide range of power-law frictions. We examine power-law exponents with $\eta = .8$, .4 and .2. We also examine slip-weakening and velocity-weakening frictions. All of these frictions are plotted in Plate 5; the different colors differentiate the different frictions, with the cold colors (blue, green, and cyan) representing slip-weakening and the hot colors (red, magenta, and black) representing velocity-weakening. We have used the same symbols for the same exponents η for the slip-weakening and the velocity-weakening frictions. On this plot, nonlinear scaling is apparent. The cause of this scaling, however, is not. To explore that, we need to look at the events in other ways as well.

The plot we find most clear in elucidating the nonlinear scaling is made in Plate 6, where we plot apparent stress $\tau_a = E_R/M$ versus the length of the rupture L. We see both small events breaking lengths less than the seismogenic crust depth length unity $L < 1$ and large events breaking $L > 1$. Both have little size dependence. Some size dependence can be seen in the intermediate sized events when the small and large events differ in τ_a, as the intermediate sized events interpolate between the small and large events. This result is surprising, since the power law slip-weakening was explicitly constructed to give an η dependent increase of τ_a at all lengthscales [*Abercrombie and Rice*, 2005]. Since it is quite unexpected, we will return to this issue again. Two aspects of the small events are clear in this plot: the different color symbols overlay, while the different symbols do not. That is, the exponent of the power-law η affects the amplitude of τ_a while the type of instability– slip-weakening versus velocity-weakening– does not affect the amplitude of τ_a.

We want to examine as a potential cause of anomalous τ_a scaling the possibility that the static stress drop $\Delta\tau$ might be changing and driving the τ_a behavior. While in earthquakes measured $\Delta\tau$ values suggest it is remarkably constant across a the whole range of earthquake sizes [*Hanks*, 1977], different frictions can produce nonconstant $\Delta\tau$. A plot of M versus L for the events shows some slight deviations from the straight line constant-stress drop scaling for the different frictions, but the results are within the scatter of the earthquake observational data [*Hanks*, 1977]. These slight deviations are easier to see if we look at the scaling of $\Delta\tau$ directly. Plate 7 shows a plot of the average stress drop $\Delta\tau$ as a function of the rupture length L. To make this plot, we measure the stress change over the area which ruptured for each event, average that stress over the rupture area, and then group these measured stress changes into events of similar size and average over similar sized events. Subtle trends in moment-length scaling, which would typically be lost in the large scale ranges and scatter, become magnified here. One trend is quite surprising: average stress drops for small events are seen to actually be decreasing slightly with

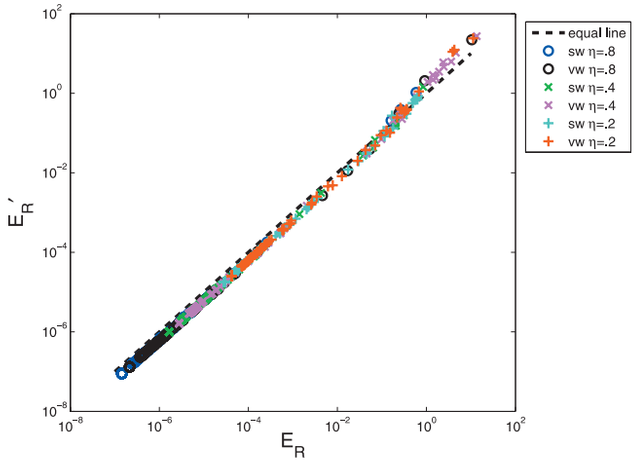

Plate 2. Kinetic energy flux E_R' versus radiated energy E_R estimated from energy conservation. Note good agreement between the two completely independent ways of measuring energy. Dashed line shows equality. There is some deviation from linearity at the largest events, due to the surface through which we are measuring kinetic energy flux being only a finite distance from the fault, so we end up with some near field excess kinetic energy, which would otherwise turn into potential energy before reaching the true far field.

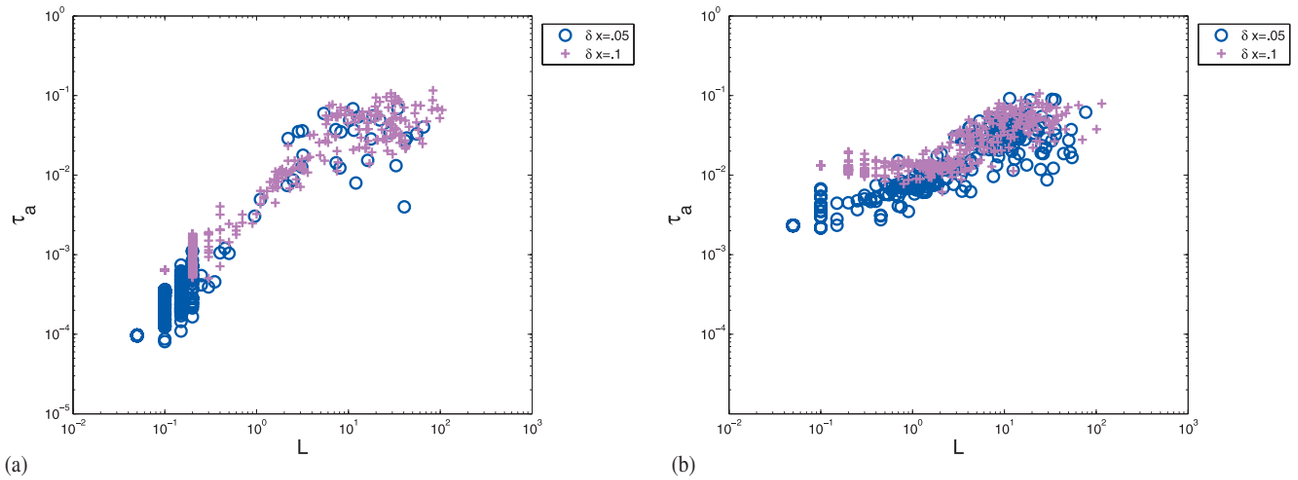

Plate 3. Apparent stress τ_a versus length of rupture L. Two different grid resolutions are shown, $\delta_x = .05$ (o) and $\delta_x = .1$ (+). (a) $\eta = 1$ continuum case; note the overlay of the symbols. (b) $\eta = .4$ noncontinuum case; note the lack of overlay in the symbols for small events.

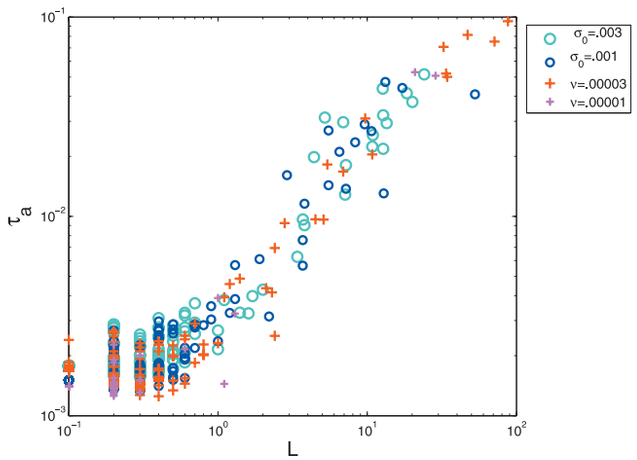

Plate 4. Apparent stress τ_a versus length of rupture L for different nucleation values and mechanisms. Note all the curves overlay, so the systematics of the change in τ_a with L are not being affected by the nucleation. The dark and light blue circles are time weakening nucleation, while the red and magenta plusses are continuous loading without a time weakening mechanism. A factor of 3 change in parameters in both mechanisms does not affect the results, nor, quite importantly, does a change in mechanism, when the relevant nucleation parameters σ_0 or ν are sufficiently small. (In order to measure radiated energy in the continuously loaded case $\nu \neq 0$, we use in just this one figure the kinetic energy flux E_R' rather than radiated energy E_R, leading to what looks like an increase in τ_a for the large events, which does not, in actuality, occur; the deviations from a straight line in Plate 2 at the largest events show the same finite flux surface distance effect).

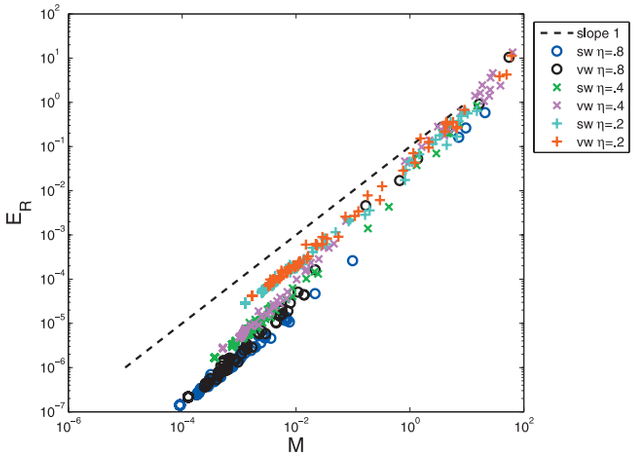

Plate 5. Radiated energy E_R on the vertical axis versus moment M on the horizontal axis, for a range of power law weakening frictions. The legend indicates the power law exponent value, along with sw indicating slip-weakening friction and vw indicating velocity-weakening friction. The dashed line has slope 1, showing what would be a linear relationship between E_R and M.

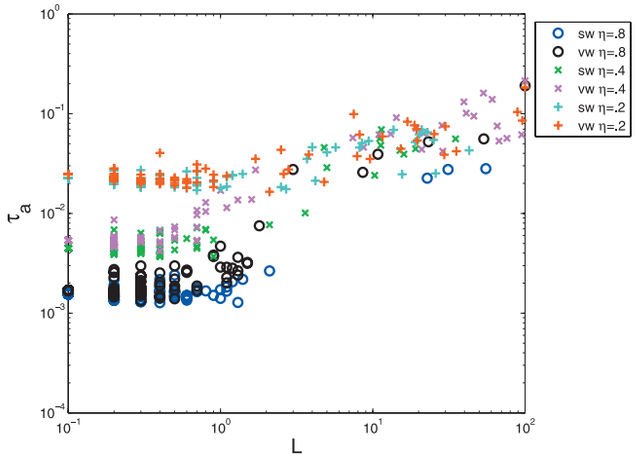

Plate 6. Apparent stress τ_a versus length of rupture L for a range of power-law frictions. Legend indicates power law exponent value and slip-weakening (sw) or velocity-weakening (vw) friction. Note similar symbols overlaying, showing little difference between slip-weakening and velocity-weakening, while different colors do not overlay, showing dependence on exponent for small events. Note, importantly, lack of increase of τ_a with L for small events $L < 1$.

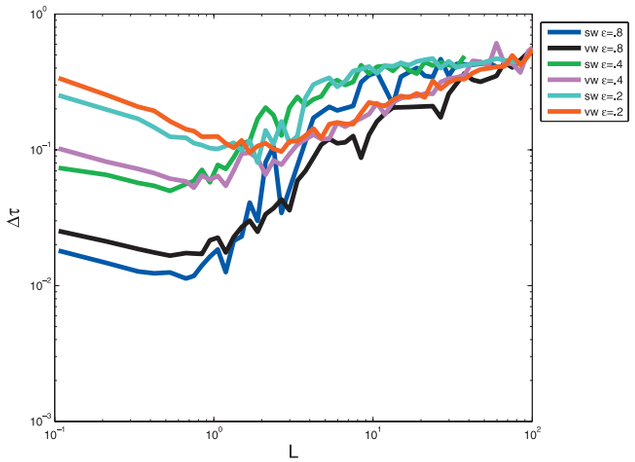

Plate 7. Average stress drop $\Delta\tau$ as a function of rupture length L for different power-law weakening frictions. The legend indicates the power law exponent value, along with sw indicating slip-weakening friction and vw indicating velocity-weakening friction. Stress drops are measured directly from slipped fault patch, then averaged over events of similar rupture length. Note the slight but surprising decrease of $\Delta\tau$ with L for small events.

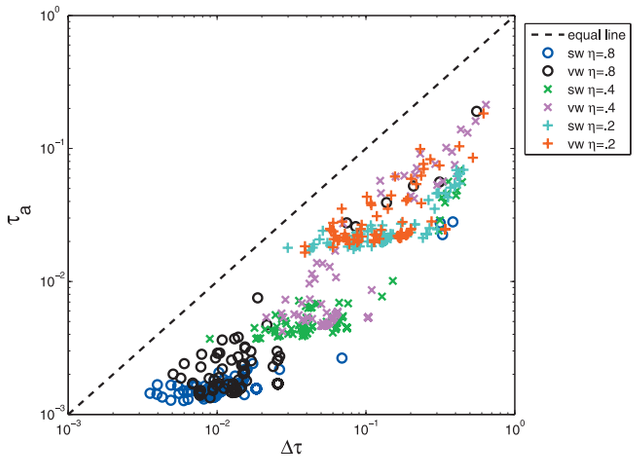

Plate 8. Apparent stress τ_a versus static stress drop $\Delta\tau = M/L^2$. Dashed line shows equality. Note generally low values of τ_a compared with $\Delta\tau$. These values seen are very reasonable compared with the observations of *Abercrombie* [1995] where τ_a is roughly a factor of 10 less than $\Delta\tau$.

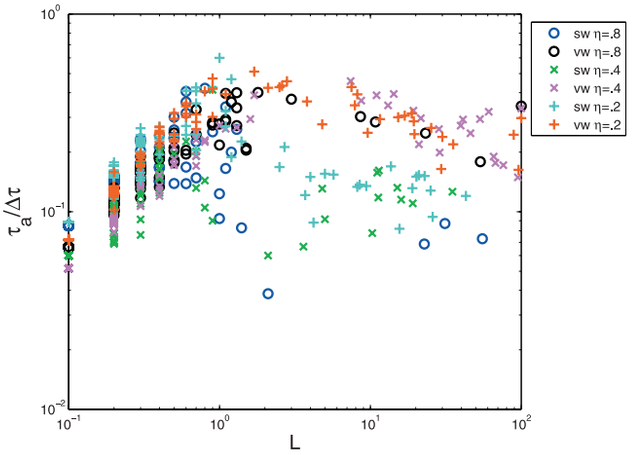

Plate 9. Dimensionless ratio $\tau_a/\Delta\tau$ versus length of rupture L. Note higher values of ratio for velocity-weakening compared to slip-weakening for large events. Note relatively little change across entire range of lengthscale.

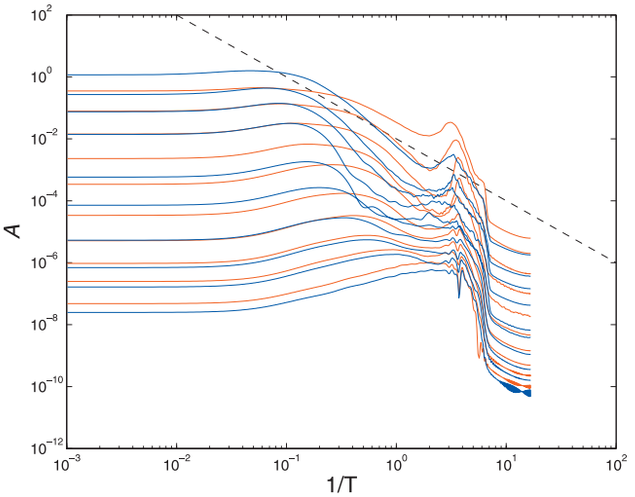

Plate 10. Average radiated energy spectra for events of different sizes, with amplitude A on vertical axis and inverse period of waves $1/T$ on horizontal axis. Red curves are velocity-weakening and blue curves are slip-weakening. Note more high frequency energy in red velocity weakening curves as compared with blue slip-weakening curves for a given moment. Dashed line has slope –2.

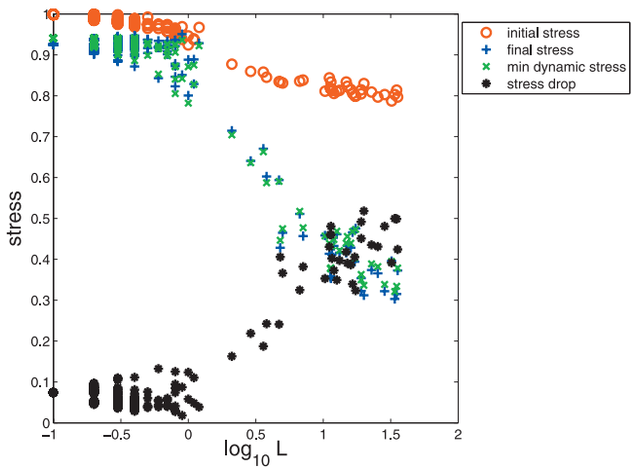

Plate 11. Average stress values over length L of event which ruptured, plotted versus L. The different symbols show stress before rupture occurred, after rupture occurred, minimum dynamic friction during rupture, and static stress drop from difference between initial and final stress. Note average initial stress decreases with increasing L, due to larger ruptures being more capable of propagating into low stress regions, an effect often neglected in simple scaling estimates.

L—the opposite as presumed for power-law weakening. We will return to examine why this is happening later. For now, note that how static stress drop scales also impacts how apparent stress scales.

They are, however, not trivially related, as a plot of τ_a versus $\Delta\tau$ shows, a plot like that made with real data by *Abercrombie* [1995]. One thing is clear for all the frictions: they emit only a small fraction of the energy change in an event. The model events are thus very "quiet". This raises an important observational question for earthquakes as to what exactly this fraction is. Other trends in the data include a relatively constant τ_a as $\Delta\tau$ decreases for the small events, but this is not so easily seen in this plot due to the mixture of different sized events. The next plot shows this more clearly.

Plate 9 plots the dimensionless ratio $\xi \equiv \tau_a / \Delta\tau$ [*Savage and Wood*, 1971] versus the length of the rupture. Here we see the role of the changing static stress drop more dramatically, which tilts the relatively level apparent stress into an increasing ξ ratio for the small events. This looks different from prior work which showed slip and velocity weakening behaving very differently in the ξ ratio for small events [*Shaw*, 1998]; that prior result is recovered if we operate with significant additional damping from velocity strengthening, but here, with low levels of damping, which should be the relevant limit, we do not see such dramatic differences in small events. It may also be that strong reflections from a nearby stiff boundary in the earlier work may be the cause of differences in the subtle source physics sensitive trends. Here, the main difference between slip-weakening and velocity-weakening seen is in the amplitude of the ratio for large events, with velocity-weakening having substantially higher ξ than slip weakening. Note that the ξ ratios in general satisfy the Savage Wood inequality [*Savage and Wood*, 1971], which says they should be less than or equal to 1/2 when the dynamic stress is not less than the final stress.

Finally we wish to look in more detail at the ruptures to try to get at some answers as to why we see such unexpected scaling for τ_a for small events. Looking at more than just the total radiated energy, we can look at the spectral content of the radiated energy. Just as we looked at the kinetic energy flux through an array of meters on a bounding surface, we can look at the spectral content of that kinetic energy, to measure the radiated energy spectra [*Shaw*, 2003]. Plate 10 shows this for both slip-weakening and velocity-weakening averaged over events of similar sizes. We see some differences in the higher amplitudes of the higher frequencies for the large events of velocity-weakening compared to slip-weakening. This disaggregation does not, however, seem to obviously answer our questions about anomalous τ_a versus L scaling.

Our final plot, Plate 11, which looks at stresses, does, however, provide some insight. For each event, we plot stresses averaged over the length of fault which broke, versus the length of the event. A set of stresses, relevant to the energetics, are shown. These stresses are all quite heterogenous, having evolved over time as many previous ruptures have broken the fault. We get a single value for a particular stress, say the initial stress τ_1, by keeping track of the stress prior to a given event, and then after the event is over, averaging the stress prior to that event over the length L of the fault which ruptured in that event. Note also, as mentioned earlier in the modeling section, only strength drops, not absolute strength, even heterogeneous absolute strength, matters in the problem [*Shaw*, 2004]. Thus the initial stress values also act as the strength excess in the problem. In Plate 11 the threshold stress is unity, and the initial stress, minimum dynamic stress, and final stress are all seen to fall below that threshold. Note a very clear and significant trend in the initial stress: the average initial stress is dropping as the events get larger, so a smaller fraction of the dynamic stress drop is available to contribute energy to radiate. This scale dependence of initial stress can be understood for the following reason. Because ruptures initially start at places which are at the threshold breaking strength, the strength excess, or difference between the threshold strength and initial stress, will vanish there. Neighboring regions, having not spontaneously nucleated a rupture themselves, will be below threshold, and have some nonzero strength excess. Averaging over all the area which ruptured in an event will give some average strength excess value. Since larger ruptures carry more kinetic and potential energy with them, they are capable of breaking less stressed– more stuck– regions. Thus, in a heterogeneous stress context, we find that larger events tend to break regions which, on average, have lower initial stress. This affects both the energy available to radiate, and the static stress drop, causing the unexpected scaling with L we see for τ_a and $\Delta\tau$ for power-law weakening. Thus we see that arguments seeking to derive radiated energy and static stress drop scaling from friction laws will need to account for these potential scale dependent stress effect, which have strongly affected the scaling we have seen here.

4. CONCLUSIONS

We have examined how radiated energy scales with moment, with a particular focus on frictions which weaken as a power-law function of slip or slip-rate. This was motivated by the suggestion [*Abercrombie and Rice*, 2005] that increases in the radiated energy-moment ratio with increasing moment could be explained by power-law slip-weakening. While we are not able to obtain a continuum limit due

to singularities introduced by the power-law weakening, for the frictions we have examined we have not found evidence that this mechanism works; in particular, we do not see an increase in apparent stress with moment at all length scales for power-law slip-weakening. We have verified our methodology with directly measured kinetic energy flux and conservation of energy methods. For radiated energy versus moment, we have found scaling contrary to expectations from simple fracture energy arguments [*Abercrombie and Rice*, 2005]. We have traced the issue to assumptions about initial stress, with systematic scale dependent changes in average initial stress and final stress as a function of rupture size found in our models. *Abercrombie and Rice* [2005] did not consider the possibility of a systematic scale dependence of initial stress, and such an effect, which we have found here numerically, would indeed impact their results. This illustrates the need to consider all of the terms potentially relevant to energy and stress drop scaling arguments, and the usefulness of numerical simulation in the face of such complex nonlinear events.

Looking at the ratio of apparent stress to stress drop [*Savage and Wood*, 1971], we see an interesting friction difference in how this dimensionless ratio ξ scales with earthquake size, with slip-weakening showing smaller values compared with velocity-weakening for large events for the frictions we use here, and relatively small values seen for all sizes. This is seen to hold here for a range of power law exponents. The difference in average values for ξ for slip versus velocity-weakening points to this ratio as being an important measure of earthquakes, and one worth pursuing observationally.

Acknowledgments. The manuscript was improved by the comments of two anonymous reviewers and the editor. This work was supported by NSF grants PHY99-0794 while the author was at the KITP and grant EAR-03-37226, and by a grant from the Southern California Earthquake Center.

APPENDIX

The simulation is run using dimensionless units, so as to minimize the number of parameters. For use in comparing with the real earthquake system, however, we can also covert back to dimensionful variables. The conversion back to dimensional units is as follows.

wave speed: $c = 1 = \frac{L}{T} = 3\ km/sec$

crustal length scale: $L = 1 = 15\ km \rightarrow$

crustal time scale: $T = 1 = 5\ sec$

stress drop: $\Delta\tau = 1 = \frac{UG}{L} = 3\ Mpa \rightarrow$

large event slip: $U = 1 = \frac{\Delta\tau L}{G} = 10^{-4} L = 1.5\ m$

modulus: $G = 3 \times 10^4\ Mpa$

slip rate: $\frac{\pi U}{T} = \pi = 1\ m/sec$

slip-weakening length: $\frac{U}{\alpha} = .5\ m$

frictional healing time: $\frac{1}{\gamma} = 10T = 50\ sec$

domain size along faults: $L_x = 100L = 1500\ km$

domain size $\perp$ faults: $L_y = 12L = 180\ km$

grid resolution: $\delta_x = .1\ L = 1.5\ km$

nyquist frequency: $\frac{c}{2\delta_x} = 1\ hz$

apparent stress: $\frac{E_R}{M_0} = \frac{E_R}{GM} = \frac{\Delta\tau}{2G} = 5 \times 10^{-5}$

REFERENCES

Abercrombie, R. E., Earthquake source scaling relationships from -1 to 5 M_L using seismograms recorded at 2.5-km depth, J. *Geophys. Res., 100*, 24,015, 1995.

Abercrombie, R. E., and J. R. Rice, Can observations of earthquake scaling constrain slip weakening?, *Geophys. J. Int., 162*, 406, 2005.

Beeler, N. M., and T. E. Tullis, Constitutive relationship for fault strength due to flash-heating, *USGS Open File Report, submitted*, 2003.

Dieterich, J. H., A constitutive law for the rate of earthquake production and its application to earthquake clustering, *J. Geophys. Res., 99*, 2601, 1994.

Hanks, T. C., Earthquake stress-drops, ambient tectonic stresses, and the stresses that drive plates, *Pure Appl. Geophys., 115*, 441–458, 1977.

Heslot, F., T. Baumberger, B. Perrin, B. Caroli, and C. Caroli, Creep, stick-slip, and dry-friction dynamics—experiments and a heuristic model, *Phys. Rev. E, 49*, 4973, 1994.

Ide, S., and G. C. Beroza, Does apparent stress vary with earthquake size?, Geophys. Res. Lett., 28, 3349, 2001.

Kanamori, H., J. Mori, E. Hauksson, T. H. Heaton, L. K. Hutton, and L. M. Jones, Determination of earthquake energy-release and M(L) using terrascope, *Bull. Seismol. Soc. Am., 83*, 330, 1993.

Lachenbruch, A., Frictional heating, fluid pressure, and the resistance to fault motion, *J. Geophys. Res., 85*, 6097, 1980.

Langer, J. S., and H. Nakanishi, Models of rupture propagation II: Two dimensional model with dissipation on the fracture surface, *Phys. Rev. E, 48*, 439, 1993.

Mayeda, K., and W. R. Walter, Moment, energy, stress drop, and source spectra of western united states earthquakes from regional coda envelopes, *J. Geophys. Res., 101*, 11,195, 1996.

McGarr, A., On relating apparent stress to the stress causing earthquake fault slip, *J. Geophys. Res.*, 104, 3003, 1999.

Melosh, H. J., Dynamical weakening of faults by acoustic fluidization, *Nature, 379*, 601, 1996.

Prejean, S. G., and W. L. Ellsworth, Observations of earthquake source parameters and attenuation at 2 km depth in the Long Valley Caldera, Eatern California, *Bull. Seismol. Soc. Am., 91*, 165, 2001.

Rice, J. R., Spatio-temporal complexity of slip on a fault, *J. Geophys. Res, 98*, 9885, 1993.

Rice, J. R., Flash heating at asperity contacts and ratedependent friction, *Eos Tran. AGU, 80*, Abstract F6811, 1999.

Richardson, E., and T. H. Jordan, Seismicity in deep gold mines of South Africa: implication for tectonic earthquakes, *Bull. Seismol. Soc. Am., 92*, 1766, 2002.

Savage, J. C., and M. D. Wood, The relation between apparent stress and stress drop, *Bull. Seismol. Soc. Am., 61*, 1381, 1971.

Shaw, B. E., Frictional weakening and slip complexity on earthquake faults, *J. Geophys. Res., 100*, 18,239, 1995.

Shaw, B. E., Modelquakes in the two dimensional wave equation, *J. Geophys. Res., 102*, 27,367, 1997.

Shaw, B. E., Far field radiated energy scaling in elastodynamic earthquake fault models, *Bull. Seismol. Soc. Am., 88*, 1457, 1998.

Shaw, B. E., Magnitude dependence of radiated energy spectra: Far field expressions of slip pulses in earthquake models, *J. Geophys. Res., 108*, 2100, 2003.

Shaw, B. E., Dynamic heterogeneities versus fixed heterogeneities in earthquake models, *Geophys. J. Int., 156*, 275, 2004.

Shaw, B. E., and J. R. Rice, Existence of continuum complexity in the elastodynamics of repeated fault ruptures, *J. Geophys. Res., 105*, 23,791, 2000.

Sibson, R. H., Interactions between temperature and pore fluid pressure during earthquake faulting and a mechanism for partial or total stress relief, *Nature Phys. Sci., 243*, 66, 1973.

Stork, A. L., and H. Ito, Source parameter scaling for small earthquakes observed at the wester Nagano 800 m-deep borehole, central Japan, *Bull. Seismol. Soc. Am., 94*, 1781, 2004.

Tullis, T. E., and D. L. Goldsby, Flash melting of crustal rocks at almost seismic slip rates, *Eos Tran. AGU, 84*, Abstract S51B–05, 2003.

Wu, Z. L., Scaling of apparent stress from broadband radiated energy catalogue and seismic moment catalogue, *Earth Plan. Space, 53*, 943, 2001.

Wyss, M., and J. N. Brune, Seismic moment, stress, and source dimensions for earthquakes in the CaliforniaNevada region, *J. Geophys. Res., 73*, 4681, 1968.

B. E. Shaw, Lamont-Doherty Earth Observatory, Palisades, NY 10964. (e-mail: shaw@ldeo.columbia.edu)